Observation of solid fuel in a supersonic flowfield

J. M. Char[1] & U. K. Hsu[2]
[1]*Air Force Institute of Technology, Gangshan, Kaohsiung, Taiwan, Republic of China*
[2]*Department of Aircraft Engineering, Air Force Institute of Technology, Gangshan, Kaohsiung, Taiwan, Republic of China*

Abstract

Hypersonic vehicles will be the new-generation of aerial transport. Hence, supersonic combustor design becomes important. Many investigations have been conducted on this subject, however, they are focused on gaseous or liquid fuels combustor. The use of a solid fuel combustor can substantially decrease complexity and cost, so for certain purposes, solid fuel supersonic combustors show advantages over other fuel systems. This research adopts a shock tube, 16 meter long and with a bore of 9 cm to create a supersonic, high-temperature, and high-pressure flowfield to observe the gasification and ignition of HTPB solid fuel under different environments. Also, full-scale 3D numerical simulation is executed to enhance the comprehension of this complex phenomenon. The CFD code is based on the control volume method and the pre-conditioning method for solving the Navier-Stokes equations to simulate the compressible and incompressible coupling problem. In the tests, a HTPB slab is placed in the windowed-test section. Various test conditions generate different supersonic Mach numbers and environmental temperatures, meanwhile the HTPB slab changes its incident angles relative to the coming shock wave. Results show that when the Mach number around the slab section is beyond 1.25, the flowfield temperature can achieve above 1100K, which is higher than the HTPB gasification temperature (930K~1090K), then the gasification happens and a short-period ignition can be observed. In particular, as the slab angle is 7°, the phenomenon is more visible. This is due to the flowfield temperature increasing when the slab angle is at 7°. The comparison between test results and CFD simulation show good agreement, so the CFD results help the understanding and analysis of this complicated test event. Several pictures demonstrating the research results are shown below.
Keywords: ignition, shock tube, HTPB, scramjet, finite volume.


WIT Transactions on Modelling and Simulation, Vol 46, © 2007 WIT Press
www.witpress.com, ISSN 1743-355X (on-line)
doi:10.2495/CMEM070031

1 Introduction

With the development of the space shuttle and solar system exploration, the hypersonic high technology in aviation will play an important role in the next-generation frontier [1]. However, the engine of the hypersonic vehicle is a kind of scamjet, but the combustor inlet air is supersonic and will be much more useful and powerful than the Ramjet [2]. In the 1960's, researchers indicated that regression ratio is the key in mixer-rocket studies. For this reason, many models are developed in different combustion conditions. Marxman and Gilbert [3] consider that the optimal position of the flame should be in the top of the fuel surface, and the regression rate is the minimum in the turbulence layer of about 10-20%. Muzzy [4] also verify that the heat convection effect is very important in fuel consumption. Smoot and Price [5] indicated the fuel regression ratio is proportional to the oxidizer flow rate in 0.8 order in lower oxidizer flow rate. During the 1990s, there were lots of basic studies conducted. Greiner and Grederick [6] expressed the fuel regression ratio as proportional to the oxidizer flow rate, and the pressure fluctuation as decreasing in raising the mixed region length. Chiaverini et al. [7] indicated that the vapor temperature of the fuel surface is between 930K and 1190K according to several different HTPB composites.

In order to investigate the ignition and combustion efficiency of a supersonic combustion ramjet and simplify the components, there is a 16 meters shock tube established as shown in Fig.1. The device consists of a long tube divided into a high pressure and a low pressure section by an aluminium diaphragm. When the diaphragm is rupturing in the high pressure driver section, a series of compression waves coalesce into a single shock front which compresses and heats the high pressure region test gas to low pressure region, and creates the supersonic gas flow condition. In the shock tube, there are lots of complex phenomena including the normal shock, contact surface, expansion wave etc. We investigate the flowfield of the supersonic flow through the plate-like HTPB solid fuel under this unsteady condition. The difficult problem, however, is that it is not easy to create a supersonic condition over a length of time. The best test period is about 10 ms. Therefore, we must be carefully in experiments and operation. There are lots of shock tube wind tunnels established for research from 1950, for example: Glass and Hall [8], Lukasiewicz [9], Nagamatsu [10], Bradley [11], Soloukhin [12], etc. In fact, the wind tunnel test is very important in classical aerodynamics. However, there is not a complete understanding of the full phenomena because of the limit of the experiment. The Computational Fluid Dynamics, CFD, is a good tool to deal with the problems. In this study, both of these two methods are used. Using CFD simulates supersonic flow through the HTPB slab, and compares with the experimental data.

2 Experimental apparatus

In Fig.1, the length of a shock tube is 16m. The high pressure region is higher than 147 psi, and low pressure region is below 1 psi. A HTPB slab, 15cm(length)×3cm(spread) ×0.5cm (thickness), is placed in 14.55m from the

start point of the high pressure region. There are two pressure transducer placed in 14.55m (#1) and 14.65m (#2), separately. The initial tube temperature is 300K. To capture the reaction, a 10W pulse laser (t=50μs) and high speed CCD camera (t=200μs) is set up.

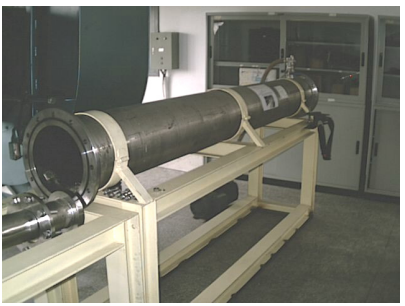

(a) high pressure section (length: 290 cm, diameter: 28.5cm)

(c) test section (window: 25cm×3cm)

(b) convergent nozzle (length: 10cm, internal diameter in divergent section: 28.5cm, internal diameter in convergent section: 9cm)

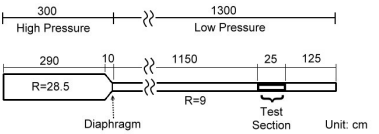

(d) dimension

Figure 1: Shock tube dimension.

3 Numerical model

Algebraically spaced grids are used to cover the flowfield, and the stretching transformation clusters using the Roberts generalized stretching transformation technique are made near the boundary layer. The Shock tube is symmetrical about the centre-plane and, therefore, only the right half of the Shock tube and plate-like model needs to be modelled. The multi-block grid approach is used in the present study. The total number of cells is 2094750 with respect to the half 3-D shock tube as shown in Fig.2. The instantaneous solution was obtained by

solving the time-dependent governing equations, and the residual is measured by the order of magnitude of the decay. The convergent solution was achieved when the residual had decayed by about 3 orders of magnitudes. Computation was performed on finer and coarser grids for a grid resolution steady; it was found that the total grid sizes, especially in the y direction, depend on the turbulence model used. According to present study, the average value of y+ closest to the surface is 0.2 with the exact solution for turbulence models [13]. The DELL OPTIPLX GX270 workstation is used for the computation.

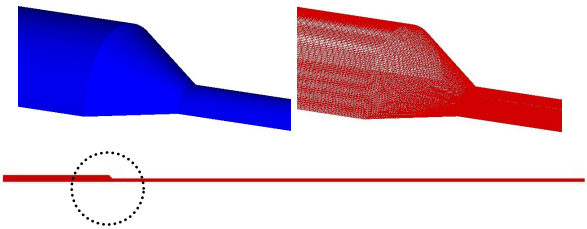

Figure 2: Longitudinal cut view of the grid system.

The numerical scheme, using the preconditioning finite volume method, is introduced to solve the governing flow equations. A 2nd-order scheme is initially applied, so the left and right states are chosen to be the cell average values on the left and right of the cell faces. In a high-resolution scheme, in order to raise the order of accuracy of upwind differencing, all one needs to do is to raise the order of accuracy of the initial-value interpolation that yields the zone-boundary data. Such schemes are labelled as high resolution schemes as opposed to Total Variation Diminishing (TVD) schemes, which completely eliminate any of those spurious oscillations when applied to one dimensional nonlinear hyperbolic conservation laws and linear hyperbolic systems. The van Leer kappa-scheme, in which the kappa number is one-third, was selected to obtain a high-resolution upwind differencing [14–16].

An optimal multi-stage scheme is used for the time integration, the multi-stage coefficients are modified by Tai et al [17] and redefined using the Courant number for multi-dimensional use. Also, a residual smoothing method is imposed to accelerate convergence and to improve numerical stability.

4 Results and discussion

4.1 Initial conditions

In order to understand the velocity and temperature statute in a shock tube, 1-D shock tube theorem is applied to determine the shock speed, temperature, and action time as following:

$$\frac{P_4}{P_1}=\frac{147(psi)}{1(psi)}=147$$

$$\because \frac{P_1}{P_4}=\frac{P_1}{P_2}\left[1-\frac{\gamma-1}{2\gamma}\frac{\left(\frac{P_2}{P_1}-1\right)}{\sqrt{1+\frac{\gamma+1}{2\gamma}\left(\frac{P_2}{P_1}-1\right)}}\right]^{\frac{2\gamma}{\gamma-1}}$$

$$so, \quad \frac{P_2}{P_1}=7.0$$

from normal shock table, it shows $M_s=2.48,$ and hence $\mathrm{M}_2=0.5149,\ T_2=635.4K$.

The history of the action time is shown in Fig.3. The main shock wave has reflected to the test model before the contact surface arrived. Therefore, the period of the test time is only 3.2 ms.

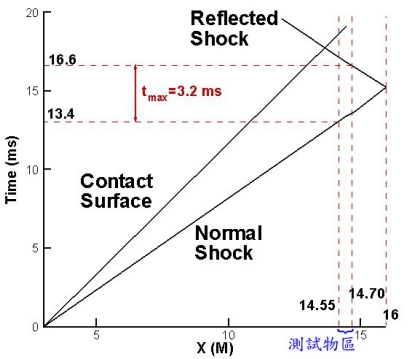

Figure 3: 1-D theorem determined result.

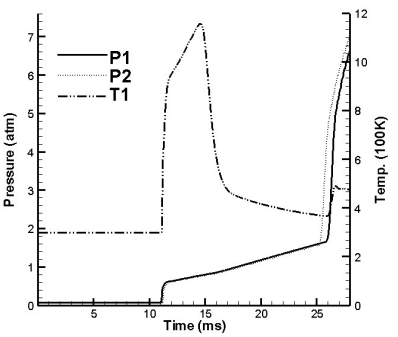

Figure 4: Pressure and temperature profile at point #1& #2.

4.2 Full-scale shock tube simulation

We can set the time step in unsteady simulation from the above 1-D theorem determined. In Fig.4, P1 and P2 are presented the position of the pressure transducer (#1 and #2) individually. The result shows the shock speed is 787.4 m/s in test section. The main shock arrived point #1 at t=11.08ms, and is faster by 2.32ms than theorem determined. The numerical model simulates the real case that the calibre is reduced to 1/3 when section is in the low pressure region from high pressure region. For this reason, the shock speed is rapidly increased. The calculation of the theory regards, in terms of the main straight tube as,

neglects the heat effect and boundary layer effect, because their response time is relatively slow if comparing with the test event interval. Fig.5 and Fig.6 show pressure and temperature change in different time steps: (a) shows the initial state after the diaphragm broken; (b) and (c) show the incident shock wave propagation phenomena. Fig.6(b) shows the temperature distribution, and a contact surface can clearly find. Fig.6(d) and 6(e) show the detail of the reflection shock wave. Because the wind tunnel is a close type, the pressure is dropped naturally in the high pressure section after the main shock released as shown in Fig.5.

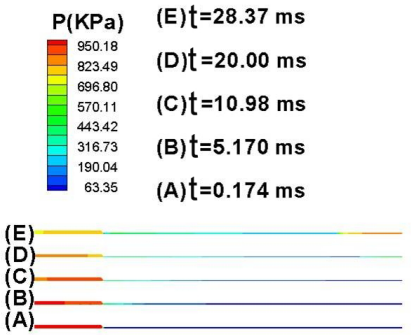

Figure 5: Snapshots of the pressure distribution in a tube.

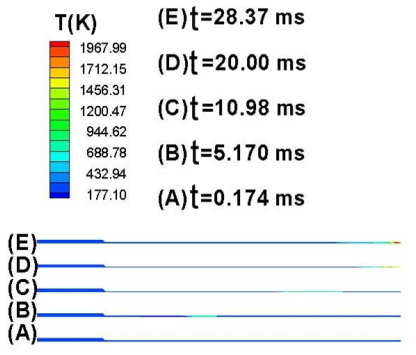

Figure 6: Snapshots of the temperature distribution in a tube.

4.3 Different fuel slab angle analysis

After understanding the phenomena of a full scale shock tube, a fuel slab is placed in test section (X=14.55~14.70M), to investigate the physical phenomena of the fuel slab surface in different angles of attack (AOA=0°, 7°, and 10°). Figs 7–9 show the slab surface pressure, temperature, and Mach number. Due to the symmetric shape across the upper and lower area of the slab at AOA=0°, the distribution curves are merged as one line. But at AOA=7° and 10°, the temperature and pressure curve across the upper and lower surface show differently in Figs 7–9. In Fig. 10, at AOA=0°, the blunt shape of the leading edge causes the supersonic bow shock, and one more shock wave is followed to make the temperature rise once again near the leading edge afterwards. The channel flow seems to be through a convergent nozzle between the upper and lower passage because of the boundary layer effect. Also, because of the passage flow wall effect, the shock wave is reflected, which makes the speed rapidly reduced. Therefore, the Mach number is decreasing from 1.25 to M=0.5 when air flow attached a reflection shock at X/C=0.1. Following on, the flow speed is raised at X/C=0.15~0.4 because of the convergent passage that the boundary layer affects.

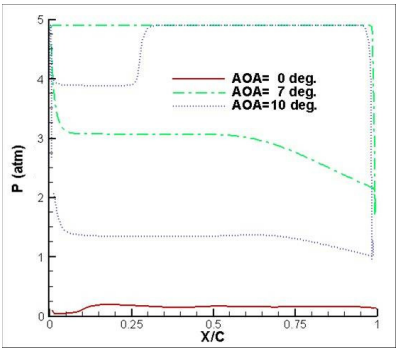

Figure 7: Pressure profile of HTPB surface in different AOA.

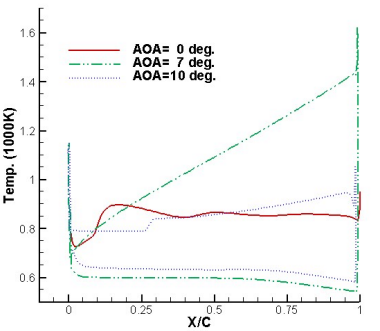

Figure 8: Temp. profile of HTPB surface in different AOA.

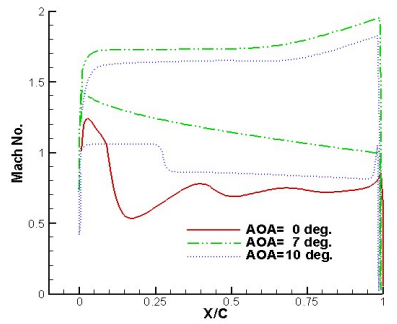

Figure 9: Mach No. profile of HTPB surface in different AOA.

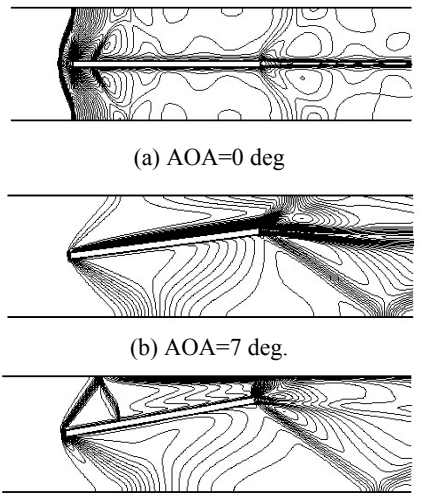

(a) AOA=0 deg

(b) AOA=7 deg.

(c) AOA=10 deg.

Figure 10: Iso-density contour.

However, the energy after the reflecting shock wave is reduced too fast, so the Mach number tends towards stability after X/C=0.5. As 7 degrees of angles of attack, the impact effect on the upper surface increases so temperature is higher than 0 degrees case. The supersonic flow will reduce speed and raise pressure because of a geometric convergent passage. The shock wave which occurred in leading edge of upper surface will reattach at the trailing edge through the reflection shock. The main shock wave has the deflection characteristic due to the decline of the slab so the air flow oppresses the boundary layer. For this

reason, the temperature is increasing on the upper surface. The supersonic flow speed raised and pressure reduced when the air flow over the lower surface which is like in a divergent nozzle. Therefore, at AOA=7° and HTPB fuel is mounted on the upper surface of the slab; high temperature helps the gasification and ignition in HTPB plate. In Fig.9, we found the air flow speed still above M=1 either on upper or low surface in AOA=7°. Therefore, this situation can satisfy the ignition in supersonic flow. As AOA=10°, the average temperature is not so good as in AOA=7°, but the speed is still above M=1. Because of the reflection of the main shock wave in the leading edge, the pressure is reduced, the temperature is raised, and Mach number is reduced after the flow through the reflection shock (Fig.7 to 9, X/C=0.3).

4.4 Experiment visualization

Fig.11 shows the time history snapshot of the shock wave using a CCD camera. The shock wave arrived to slab (AOA=7deg) at t=11.1 ms. The oblique shock has occurred because of the angle shape configuration. The secondary oblique shock wave is induced at t=11.7ms when the flow over the HTPB. Comparing with CFD results, in Fig.12, the flow speed behind the shock is kept in transonic on the upper side, and the speed of the lower side increased to M=2. Although the speed is reduced behind the oblique shock on the upper side, the temperature is also proportional to the length as shown in Fig.8.

The reflection shock is induced in the trailing edge at t=14.1ms as shown in Fig.11(d). The period is about 3 ms between the shock arrived and reflection shock attached the test section. Fig.13 shows the time history of pressure transducer record at 14.55M (#1) and 14.65M (#2). Because the HTPB fuel is not burned, the change of pressure transducer record is not clear until the hit of main shock and reflection shock. We can find the pressure fluctuation after a rapid peak as shown in Fig.13, because of the interaction of shocks in the tube. The total pressure is not reduced until the pressure goes to stable after the peak value.

It is observed that gasification exits when the shock wave goes across the HTPB. From the recovered fuel, there is a melt in the leading edge as shown in Fig.14. This region is a stagnation zone for a bow shock, where flow speed is slow and temperature is high. The temperature can reach 1100K as shown in Fig.8. The temperature has already been higher than the surface gasification temperature (930K 1190K) of HTPB, and there is enough time in the district for burning. The flow speed in other places is too fast, so the temperature has not reached the gasification criterion, and it is unable to burn.

5 Conclusion

From the numerical simulation result, the HTPB slab at an angle of attack of 7 degrees has a higher temperature and pressure in the upper surface than 0 degrees and 10 degrees, and the flow speed of the upper and lower surface keeps in supersonic flow and contributing to gasification ignition. According to the

experimental data and numerical result, the test periods are both about 3 ms, and it had the melt in the leading edge of the tested HTPB slab. In other areas, although they reach the gasification criterion, it is unable to burn because the flow speed is too fast and the test time is limited by 3ms of shock tube facility.

(a) before event (t=0 sec)

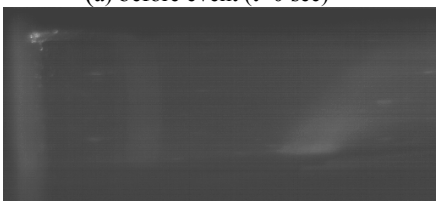

(b) shock wave arrived (dir.:➔, t=11.1ms)

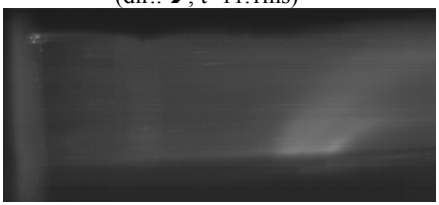

(c) shock wave through (dir.:➔, t=11.7ms)

(d) ref. Shock (dir.:➔, t=14.1ms)

Figure 11: Snapshots of shock wave.

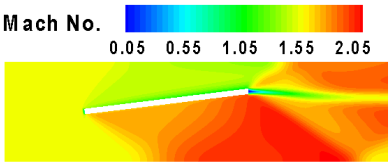

Figure 12: Mach No. distribution.

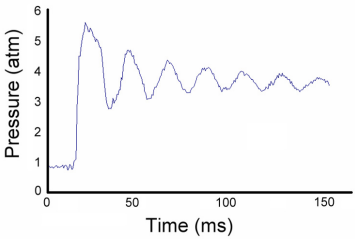

Figure 13: Pressure measurement (point#1).

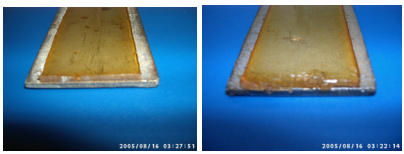

(a) (b)

Figure 14: Comparison before and after the action: (a) without action, (b) with action.

Acknowledgement

The authors are grateful to the National Science Council of the Republic of China for financial support under contract number NSC 93-2212-E- 013-007.

References

[1] Waltrup, P. J., White, M.E., Zarlingo, F., and Gravlin, E. S., "History of U.S. Navy Ramjet, Scramjet, and Mixed-Cycle Propulsion Development," Journal of Propulsion and Power, Vol.18, No.1, pp.14-27, 2000.
[2] Jones, R. A. and Huber, P.W. "Toward Scramjet Aircraft," AIAA Journal, Vol.16, pp.38-48, 1978.
[3] Marxman, C. A., and Gilbert, M., "Turbulent Boundary Layer Combustion in the Hybrid Rocket," 9th International Symposium on Combustion, Academic Press, Inc., New York, 1963, pp.371-383.
[4] Muzzy, R. J., "Applied Hybrid Combustion Theory," AIAA Paper No. 72 1143, 1972.
[5] Smoot, L. D., and Price, C. F., "Regression Rates of Nonmetalized Hybrid Fuel Systems," AIAA Journal, Vol. 3, No. 8, August 1965, pp. 1408-1413.
[6] Greiner, B. and Grederick, R. A. Jr., "Results of Labscale Hybrid Rocket Motor Investigation," AIAA Paper No. 92-3301, 1992.
[7] Chiaverini, M. J. et al., "Fuel Decomposition and Boundary Layer Combustion Processes of Hybrid Rocket Motors," AIAA Paper 95-2686, 1995.
[8] Glass, I. I., and Hall, J. G., "Shock Tubes, Handbook of Supersonic Aerodynamics," NAVORD Report 1488, Vol. 6, Section 18. (1958)
[9] Lukasiewicz, J., "Shock Tube Theory and Application," National Aeronautical Establishment, Rept. 15, Ottawa, Canada. (1952)
[10] Nagamatsu, H. T., "Shock Tube Technology and Design," Fundamental Data Obtained From a Shock-Tube Experiments," Edited by A. Feri, pp. 86-136, Pergamon Press. (1961)
[11] Bradley, J. N., "Shock Waves in Chemistry and Physics," Methuen & Co. (London), J. Wiley & Sons (New York). (1962)
[12] Soloukhin, R. I., "Shock Waves and Detonation in Gases," State Publishing House of Physical-Mathematical Literature, Moscow; English Translation Published by Mono Book Corp., Baltimore. (1966)
[13] Wilcox, D. C., "Comparison of Two-Equation Turbulence Models for Boundary Layers with Pressure Gradient", J of AIAA, Vol.31, No.8, pp.1414-1421 (1993)
[14] Van Leer, B., "Upwind-Difference Methods for Aerodynamic Problems Governed by the Euler Equations, in Large-Scale Computations in Fluid Mechanics," Lectures in Applied Mathematics, Vol. 22, pp. 327-336(1985).
[15] Roe, P. L., "Approximate Riemann Solvers, Parameter Vector, and Difference Schemes," Journal of Computational Physics, Vol. 43, pp.357-372(1981).
[16] Edwards J.R. and Liou M. S. "Low-Diffusion Flux-Splitting Methods for Flows at All Speeds" AIAA J., Vol.36. No.9, 1610-1617, (1998).
[17] Tai, C. H., Sheu, J.H, and van Leer, B., "Optimally Multi-Stage Schemes for the Euler Equations with Residual Smoothing," Journal of AIAA, Vol.33, No.6, pp.1008-1016 (1995).